Petroleum Science 23 (2026) 5509–5523

Contents lists available at ScienceDirect

Petroleum Science

journal homepage: www.keaipublishing.com/en/journals/petroleum-science

Original Paper

Impacts of temperature and pressure on light hydrocarbon parameters during gas washing: Results from simulation experiments

Wen-Na Liu [a,b,c], Wang-Lu Jia [a,b,*], Qiang Wang [a,b], Jian Chen [a,b], Jin-Bu Li [a,b], Ping-An Peng [a,b,c]

[a] State Key Laboratory of Deep Earth Processes and Resources, Guangzhou Institute of Geochemistry Chinese Academy of Sciences, Guangzhou, 510640, Guangdong, China
[b] CAS Center for Excellence in Deep Earth Science, Guangzhou, 510640, Guangdong, China
[c] University of Chinese Academy of Sciences, Beijing, 100049, China

ARTICLE INFO

Article history:
Received 7 July 2025
Received in revised form
13 December 2025
Accepted 12 March 2026
Available online 18 March 2026

Edited by Min Li

Keywords:
Gas washing
Temperature and pressure
Light hydrocarbon parameters

ABSTRACT

As a secondary alteration process in oil reservoirs and a critical mechanism for light oil and condensate formation, gas washing is predominantly governed by temperature and pressure. However, the dynamic effects of these two factors on the light hydrocarbon composition of residual oil remain unclear. This study developed a methane-pressurized gas washing simulation apparatus that can maintain predetermined pressure and temperature conditions throughout the experiment. The aim of this study is to investigate the variation patterns of light hydrocarbons under different temperature and pressure conditions, and to further evaluate their potential influences in identifying the type and depositional environments of source organic matter, quantifying thermal maturity, and identifying secondary alteration processes. By establishing the relationship between the remaining mass fraction of light hydrocarbons and time, the loss rate constants for individual components were obtained. Comparative analysis revealed that the loss rates of light hydrocarbons increased significantly with rising temperature during gas washing, but were suppressed with increasing pressure. Among the parameters indicative of source rock type and depositional environment, the Mango parameter K_1 and the C_7 ternary diagram were less affected by gas washing and changes in temperature and pressure. In contrast, parameter K_2 and Halpern's oil-gas correlation parameters (C_7-OCSD star diagram) underwent considerable alterations. Gas washing resulted in an increase in both MCH/(MCH + nC_7) and Tol/(Tol + MCH) ratios, a trend opposite to that induced by increasing maturity. Furthermore, elevated temperature significantly promoted an increase in the MCH/(MCH + nC_7) ratio, whereas increased pressure exerted an inhibitory effect on this ratio. The variation in secondary alteration parameters (Tol/nC_7 and nC_7/MCH) is consistent with classical theory: gas washing leads to an increase in Tol/nC_7 and a decrease in nC_7/MCH. Furthermore, higher temperatures result in a smaller increase in Tol/nC_7, while greater pressure leads to a more pronounced increase. These findings enhance the understanding of how temperature and pressure govern gas washing mechanisms, providing critical insights for more accurately identifying hydrocarbon origin, maturity, and secondary alteration processes in complex geological contexts.

1. Introduction

As global oil and gas exploration moves toward deep and ultra-deep reservoirs, light oil and condensate have become key targets (Tuo, 2002; Wu et al., 2025; Zhang et al., 2015). These fluids usually exist under high-temperature and high-pressure conditions and have complex origins (Zhu et al., 2020, 2022). Their formation is often linked to high thermal maturity, oil cracking, or gas washing. Light hydrocarbons (LHs, C_5–C_{12}) constitute the major components

* Corresponding author.
E-mail address: wljia@gig.ac.cn (W.-L. Jia).
Peer review under the responsibility of China University of Petroleum (Beijing).

https://doi.org/10.1016/j.petsci.2026.03.031

of light oil and condensates (Halpern, 1995; Mango, 1987, 1997, 2000; Philippi, 1975; Thompson, 1988). Owing to their high volatility and sensitive geochemical responses, LHs act as crucial indicators for tracing oil origin, determining thermal maturity (Deng et al., 2023; Rabbani et al., 2023), and identifying post-generation alterations (e.g., gas washing, evaporative fractionation, and biodegradation; Hu et al., 2014; Huang et al., 2023; Thompson, 1987).

Evaporative fractionation alters the LH composition of oil (Thompson, 1987) and further affects the characteristics of LH parameters. Simulation experiments reveal that loss rates of C_5–C_8 hydrocarbons are controlled by molecular weight and structure: *n*-alkanes' volatility decreases with increasing carbon number. Among C_7 compounds, volatility follows branched alkanes > *n*-heptane > methylcyclohexane > toluene (Bouchard et al., 2008; Liu et al., 2024; Xiao et al., 2012). This fractionation can systematically bias volatility-sensitive parameters and lead to misinterpretations of oil's formation conditions. Notably, while Mango's (1987) steady-state catalytic parameters (e.g., K_1 = (2-methylheptane+2,3-dimethylpentane)/(3-methylheptane+2,4-dimethylpentane), K_2 retain strong correlation ($R^2 > 0.9$) during volatilization, the 2,4-dimethylpentane/2,3-dimethylpentane (2,4-DMP/2,3-DMP) ratio thermometer exhibits a systematic underestimation of 5–15 °C due to evaporative fractionation effects (Cañipa-Morales et al., 2003). For identifying secondary alterations, the two-parameter discrimination system proposed by Thompson (1987), which combines the toluene/*n*-heptane (Tol/nC$_7$) and *n*-heptane/methylcyclohexane (nC$_7$/MCH) ratios, exhibits distinct responses to volatilization: aromatic (Tol) and cycloalkane (MCH) compounds become enriched in the residual liquid, whereas *n*-alkanes are preferentially partitioned into the vapor phase. This process alters the original molecular composition in a systematic manner, producing characteristic directional trends in Tol/nC$_7$ and nC$_7$/MCH ratios in affected reservoirs. These shifts thus serve as reliable diagnostic markers for evaporative fractionation. Furthermore, Halpern's (1995) star diagram, used for oil classification, shows consistent shapes for oils of common origin. However, volatilization decreases parameters C_1, C_3, C_4 and increases C_2, C_5, potentially causing misclassification (Cañipa-Morales et al., 2003).

In addition to evaporative fractionation, thermal maturity and thermochemical sulfate reduction (TSR) are also key secondary processes that regulate the composition of LHs. With increasing maturity, *n*-alkanes tend to become relatively enriched due to their higher thermal stability, while cycloalkanes gradually decrease as ring cleavage generates low-molecular-weight alkanes. This is typically manifested by a synchronous increase in heptane value and iso-heptane value (Huang et al., 2023; Xiao et al., 2011). TSR occurs in high-temperature reservoirs and reshapes the composition of LHs through redox reactions between sulfate and hydrocarbons (Cai et al., 2022; Goldstein and Aizenshtat, 1994; Machel, 2001). Experimental simulations have demonstrated that TSR promotes the cracking of long-chain alkanes into C_6–C_7 *n*-alkanes, accelerates the isomerization of cycloalkanes, and leads to an increase in the concentration of aromatic hydrocarbons such as Tol. These changes can render some LH parameters ineffective. For example, in the Thompson parameter, the paraffinicity (nC$_7$/MCH) increases due to the enrichment of *n*-alkanes. The Mango parameter (e.g., K_1) significantly increases, and parameters such as N2 (is equal 1,1-dimethylcyclopentane (DMCP) +1,3-DMCP (*cis* + *trans*)) and P2 (is equal 2-MH+3-MH) are no longer suitable for oil-source correlation (Sun et al., 2025).

Gas washing is a common geological process in the secondary alteration of oil reservoirs and is also an important mechanism for the formation of light oil and condensate (Chen et al., 2017; Thompson, 1987; Zhang and Huang, 2005; Zhang et al., 2022). When natural gas invades an oil reservoir, it extracts the LH components from the oil. This process occurs under the high-temperature and high-pressure conditions, and generally follows the basic principles of evaporative fractionation (Li et al., 2025; Su et al., 2004). This process significantly affects the properties and compositions of oil and gas (Cai et al., 2024; Losh et al., 2002). For example, after gas washing, the relative content of nC$_7$ in residual oil decreases, while the relative contents of Tol increase (Su et al., 2000; Thompson, 1988), and the content of cycloalkane also relatively increases (Zhang et al., 2011). In recent years, the impact of temperature and pressure conditions on the oil has increasingly attracted attention. Based on PVT phase experiments, previous studies have extensively investigated gas washing in typical oil basins, providing crucial qualitative descriptions (Chen et al., 2019; Liang et al., 2010). However, conventional experimental methods typically operate under constant temperature and pressure conditions, failing to fully simulate the effects of continuously changing pressure gradients on the molecular composition of oil. Furthermore, while these methods analyze LHs by capturing gaseous products, gas washing is a multi-stage process in which characterizing the residual oil phase is equally critical.

In this study, we designed an experimental apparatus to simulate gas washing processes. This apparatus can systematically investigate the effects of variable temperature and pressure on LH geochemical parameters, focusing on two core categories: (1) parameters indicative of source organic matter and depositional environment; (2) parameters reflecting thermal maturity and secondary alteration intensity. It should be noted that the experimental pressure range utilized in this study (0.2–0.8 MPa) is constrained by the available equipment and is substantially lower than the pore fluid pressures in deep reservoirs (on the order of tens of MPa). Nevertheless, elucidating the mechanistic behavior and evolutionary trends under these low-pressure conditions offers valuable foundational insights into molecular-scale processes and provides critical input parameters for numerical modeling and theoretical extrapolation to higher-pressure environments.

2. Experiments

2.1. Experimental set-up

The setup for simulating gas washing comprises four principal components (Fig. 1): (1) a gas supply system, (2) a sample

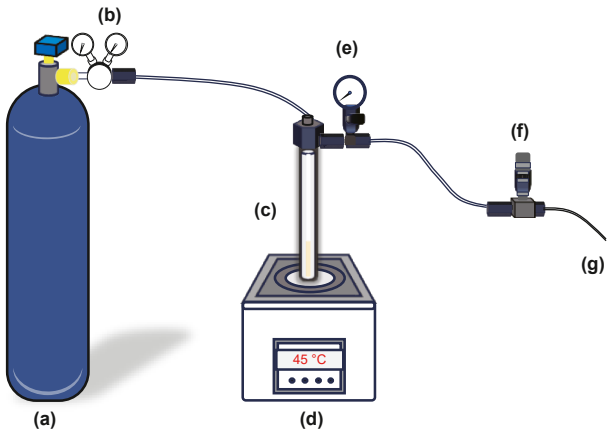

Fig. 1. Schematic diagram of the experimental setup for simulating gas washing processes.

container, (3) a temperature control unit, and (4) a flow regulation module. The gas supply system employs a 40-L high-pressure steel cylinder (a) charged with methane (CH_4) at a maximum pressure of 15 MPa. A precise pressure regulator (b) was installed at the cylinder outlet to maintain stable gas delivery. The sample container consists of a dual-chamber configuration: an inner quartz reactor tube (c) (20 cm length × 6 mm inner diameter × 3 mm wall thickness) for housing oil samples, enclosed within a stainless-steel protective sleeve to ensure safety. A high-precision pressure gauge (e) is installed at the container outlet to monitor the reaction pressure in real-time, showing good consistency with the output pressure from the pressure regulator (b). For temperature control, a water-bath heating device with a temperature controller (d) is used to achieve precise temperature stabilization of the sample container. The gas flow rate is adjusted by a flow control valve (f) mounted at the end of the system, with real-time monitoring enabled by a digital flow meter at the outlet (g). All components were interconnected using 316-grade stainless steel tubing (3 mm OD, 0.5 mm wall thickness).

2.2. Simulation experiments

The research sample, a condensate oil from the Tarim Basin, was sourced from the Early Cretaceous lacustrine hydrocarbon source rocks in the Kuqa Depression (Wang et al., 2024). In this study, three sets of experimental conditions were designed using this sample to systematically evaluate the effects of temperature and pressure on LH behavior during gas washing:

Series I (ambient pressure evaporation): Approximately 4 mL of light oil was placed in a sample vial and subjected to controlled evaporation at 35, 45, 60, and 80 °C under ambient pressure. Sampling time intervals were carefully selected to ensure a progressive reduction in residual oil volume, with ≥6 time points (see table in Supplementary Information) per temperature. At each interval, 50 ± 2 μL of sample was collected into a 2-mL vial and immediately diluted with *n*-pentane to minimize LH volatilization.

Series II (constant-pressure (0.2 MPa) gas washing): The container was pressurized (0.2 MPa) with methane (CH_4) at a constant flow rate of 6.5 ± 0.5 mL/min. Light oil samples (filling ~20% of the tube length to ensure consistent gas-liquid contact) were exposed to 45, 60, and 80 °C for varying durations (≥6 time points per temperature, see Supplementary Information), with independent samples for each time interval). Residual samples were transferred to 2-mL vials, and stored at low temperature to prevent further evaporation.

Series III (constant-temperature (45 °C) gas washing): Under isothermal conditions (45 °C), the CH_4 flow rate was also maintained at 6.5 ± 0.5 mL/min under three pressure conditions (0.2, 0.4, and 0.8 MPa). The container was loaded with oil (filling ~20% of the tube length to ensure consistent gas-liquid contact). After exposure (≥6 time points per pressure, see Supplementary Information), samples were stored at low temperature in 2-mL vials for subsequent analysis.

2.3. Gas chromatography

Gas chromatography (GC) analysis was performed using an Agilent 7980A gas chromatograph equipped with a HP-PONA capillary column (50 m × 0.20 mm i.d. × 0.50 μm film thickness) and a flame ionization detector (FID). The injector and detector temperatures were set at 300 °C. Nitrogen was used as the carrier gas with a flow rate of 0.8 mL/min and a split ratio of 10:1. The temperature program was set as follows: isothermal at 35 °C for 20 min, followed by a temperature ramp of 2 °C/min to 70 °C, and then 4 °C/min to 300 °C, held for 20 min. This experiment exhibited negligible impact on the long-chain *n*-alkanes within the sample. Consequently, high-molecular-weight *n*-alkanes were selected as standards for determining residual compound concentrations. For this purpose, *n*-tetracosane (nC_{24}) was employed as an internal standard compound to determine the residual mass fraction of LHs in the remaining sample (Fig. 2). The specific methodology is detailed in our previously published work (Liu et al., 2024).

2.4. Light hydrocarbon loss rate

To compare loss rates of different compounds during gas washing, the time-dependent residual mass fraction curves from all experiments were modeled with optimal fitting equations (Eq. (1)). This empirical model not only effectively characterizes the loss behavior of volatile organic compounds (VOCs), but also demonstrates an exponential decay pattern consistent with typical volatile substance dissipation behavior described in the ASTM (2001) standard.

$$y = a + b \cdot e^{-kx} \tag{1}$$

where a and b are empirical constants, e denotes the base of the natural logarithm, and k represents the rate constant whose magnitude directly correlates with volatilization kinetics. The model demonstrated excellent goodness-of-fit ($R^2 > 0.99$) across all experiments (Fig. 3(a)), confirming its validity in characterizing kinetic behavior during gas washing processes. Comparative analysis revealed that larger k values correspond to faster loss rates.

3. Results

Light hydrocarbons (LHs) with low initial concentrations in the oil—including 2,2-dimethylpentane (2,2-DMP), 2,4-dimethylpentane (2,4-DMP), 3,3-dimethylpentane (3,3-DMP), 2-methylhexane + 2,3-dimethylpentane (2-MH+2,3-DMP), 1,1-dimethylcyclopentane (1,1-DMCP), 1,3-dimethylcyclopentane (1,3-DMCP), and 3-ethylpentane + 1,2-dimethylcyclopentane (3-EP+1,2-DMCP)—exhibited faster depletion rates (Fig. 2). As anticipated, the complete loss of these highly volatile compounds resulted in a significant relative enrichment of less volatile components, namely *n*-heptane (nC_7), methylcyclohexane (MCH), and toluene (Tol).

3.1. Light hydrocarbon loss rates under different temperature conditions

The experimental data indicated that the loss rates of LHs increase remarkably with rising temperature. For instance, in the ambient-pressure evaporation system (Series I), the loss rate constant (k) of nC_7 increased significantly from 0.02 to 0.17 as the temperature rose from 35 °C to 80 °C (Table 1). Similarly, under pressurized condition (Series II, 0.2 MPa), the k value of nC_7 reached 0.39 at 80 °C, compared to 0.17 at 60 °C and 0.09 at 45 °C (Table 1, Fig. 3(a)).

Furthermore, for structurally similar compounds, the temperature effect becomes weakened with increasing carbon number. Take nC_6 and nC_7 as examples (Fig. 3(b), Table 1), at ambient pressure (Series I), when the temperature rises from 45 to 80 °C, the k of nC_6 increases from 0.20 to 0.53 ($\Delta k/\Delta T = 9.5 \times 10^{-3}$ °C^{-1}), and that of nC_7 rises from 0.03 to 0.17 ($\Delta k/\Delta T = 3.9 \times 10^{-3}$ °C^{-1}). Under 0.2 MPa, with the same temperature increase (45 to 80 °C), the k value of nC_6 goes from 0.25 to 0.93 ($\Delta k/\Delta T = 19.6 \times 10^{-3}$ °C^{-1}), while that of nC_7 increases from 0.09 to

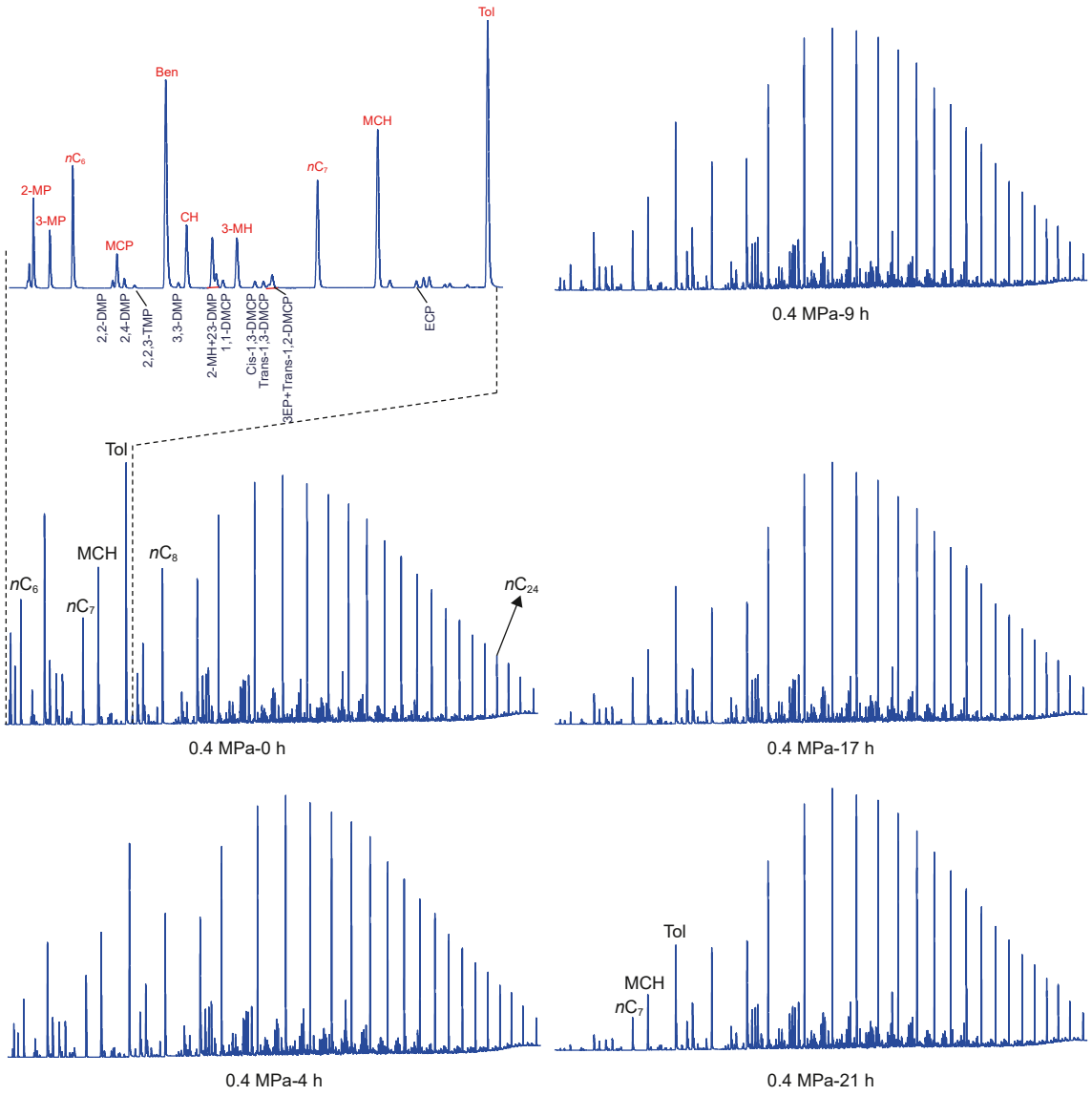

Fig. 2. Gas chromatograms of residual oil at different times under 0.4 MPa (45 °C) conditions. MP: methylpentane; DMP: dimethylpentane; nC_6: *n*-hexane; MCP: methylcyclopentane; Ben: benzene; CH: cyclohexane; MH: methylheptane; DMCH: dimethylcyclohexane; ECP: ethylcyclopentane.

0.39 ($\Delta k/\Delta T = 8.5 \times 10^{-3}$ °C^{-1}). A similar trend is observed for cycloalkanes (Table 1). For cycloalkanes, at ambient pressure, when the temperature increases from 45 to 80 °C, the *k* value of CH rises from 0.10 to 0.32 ($\Delta k/\Delta T = 6.3 \times 10^{-3}$ °C^{-1}), and that of MCH increases from 0.03 to 0.14 ($\Delta k/\Delta T = 3.1 \times 10^{-3}$ °C^{-1}). Under 0.2 MPa, within the same temperature range, the *k* value of CH increases from 0.16 to 0.60 ($\Delta k/\Delta T = 12.6 \times 10^{-3}$ °C^{-1}), and that of MCH rises from 0.08 to 0.34 ($\Delta k/\Delta T = 7.4 \times 10^{-3}$ °C^{-1}).

Analysis of compounds with identical carbon numbers further revealed distinct patterns in temperature sensitivity, with cycloalkanes consistently exhibiting the smallest response to increasing temperature (Fig. 3(b), Table 1). For C_6 compounds (3-MP, nC_6, Ben and CH), during ambient pressure (Series I), as the temperature increases from 45 to 80 °C, the order of their rate constant temperature coefficients is 3-MP ($\Delta k/\Delta T = 10.3 \times 10^{-3}$ °C^{-1}) > nC_6 (9.5×10^{-3} °C^{-1}) > Ben (7.7×10^{-3} °C^{-1}) > CH (6.3×10^{-3} °C^{-1}). For C_7 compounds (3-MH, nC_7 and MCH), the order of temperature sensitivity is 3-MH (4.9×10^{-3} °C^{-1}) > nC_7 (3.9×10^{-3} °C^{-1}) > MCH (3.1×10^{-3} °C^{-1}). Notably, the CH (C_6) and MCH (C_7) demonstrated the lowest coefficients within their respective groups, confirming their reduced thermal sensitivity. Furthermore, an interesting structural comparison emerged: toluene (Tol), characterized by a methyl group attached directly to a benzene ring, exhibited a smaller variation in loss rate with temperature compared to MCH, despite both being C_7 species. This observation underscores the significant influence of molecular structure. The pattern of influence of temperature and pressure conditions on LH loss rates is closely aligned with the results of our research team's previous study on ambient temperature evaporation (Liu et al., 2024).

3.2. Light hydrocarbon loss rates under different pressure conditions

Unlike the effect of temperature, increasing pressure had an inhibitory effect on the loss rates of LHs. For example, in the case of nC_7, under constant temperature conditions (Series III), the loss rate constant (*k*) of nC_7 decreased from 0.09 to 0.08 (a reduction of 13.9%) as the pressure increased from 0.2 to 0.8 MPa (Fig. 3(b); Table 1). Notably, no significant difference was observed between the groups at 0.4 and 0.2 MPa (Δk < 3%), which may be

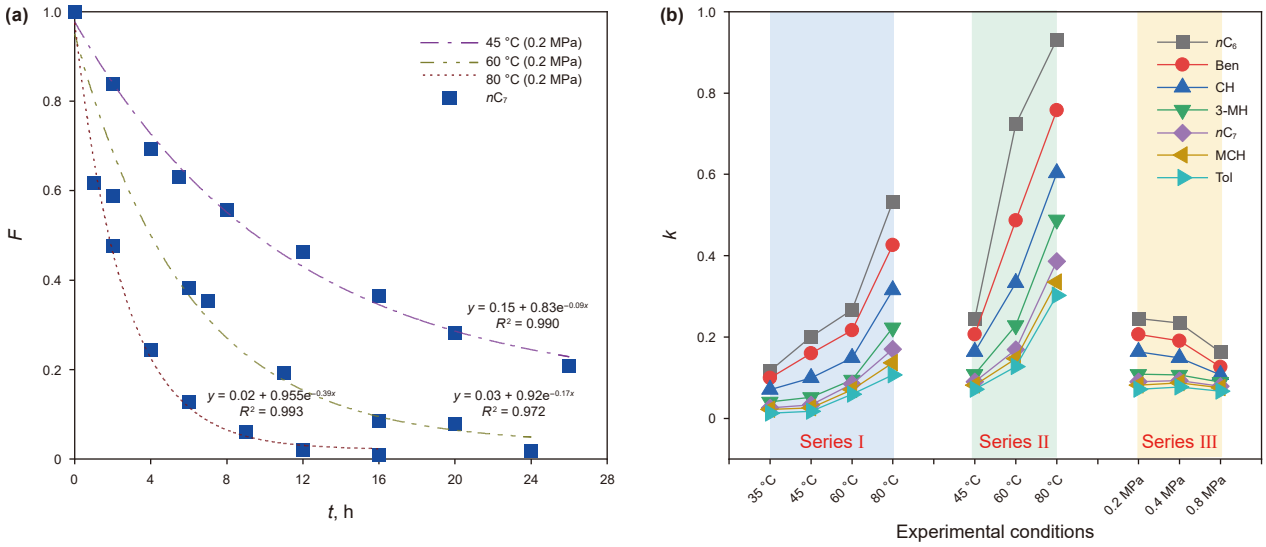

Fig. 3. (**a**) The relationship between the residual mass fraction (F) and time (t) of n-heptane (nC_7) under different experimental conditions. **(b)** The loss rates constant (k) of light hydrocarbons obtained using different experimental schemes.

Table 1
Loss rate constant k of light hydrocarbons in the three series of simulation experiments.

Compounds	Series I				Series II			Series III		
	35 °C	45 °C	60 °C	80 °C	45 °C	60 °C	80 °C	0.2 MPa	0.4 MPa	0.8 MPa
3-MP	0.13	0.29	0.31	0.65	0.32	0.88	1.05	0.32	0.30	0.20
nC_6	0.12	0.20	0.27	0.53	0.25	0.72	0.93	0.25	0.23	0.16
Ben	0.10	0.16	0.22	0.43	0.21	0.49	0.76	0.21	0.19	0.13
CH	0.07	0.10	0.15	0.32	0.16	0.33	0.60	0.16	0.15	0.11
3-MH	0.04	0.05	0.10	0.22	0.11	0.23	0.49	0.11	0.11	0.09
nC_7	0.02	0.03	0.08	0.17	0.09	0.17	0.39	0.09	0.09	0.08
MCH	0.02	0.03	0.07	0.14	0.08	0.15	0.34	0.08	0.09	0.08
Tol	0.01	0.02	0.06	0.11	0.07	0.13	0.30	0.07	0.08	0.07

attributed to the insufficient pressure gradient in the experimental design. Compared to ambient pressure at the same temperature, the loss rate of the same compound is faster at an applied pressure of 0.2 MPa due to methane purging. For instance, nC_6 at 0.2 MPa (60 °C) has a rate constant k of 0.72, higher than at atmospheric pressure (60 °C, 0.27).

Similar to Series I and II experiments, the effect of pressure on the reaction rate diminishes for compounds with high carbon numbers. For branched chain alkanes, 3-MP (C_6) exhibits a greater change in the loss rate constant k than 3-MH (C_7). As the pressure increases from 0.2 to 0.8 MPa, the k value of 3-MP decreases from 0.32 to 0.20 ($\Delta k/\Delta P = 0.20$ MPa^{-1}), while the k of 3-MH decreases from 0.11 to 0.09 ($\Delta k/\Delta P = 0.03$ MPa^{-1}). The change in the loss rate constant k of nC_6 is more pronounced than that of nC_7: when the pressure increases from 0.2 to 0.8 MPa, the k value of nC_6 decreases from 0.25 to 0.16 ($\Delta k/\Delta P = 0.15$ MPa^{-1}), whereas the k value of nC_7 decreases from 0.09 to 0.08 ($\Delta k/\Delta P = 0.02$ MPa^{-1}) (Fig. 3(b); Table 1). Hence, when the pressure change gradient is small, low-molecular - weight compounds, compared to high - molecular - weight light alkanes, tend to exhibit clearer variation. For compounds with the same carbon number, the effect of pressure on cycloalkanes is minimal. For the C_6 compounds (3-MP, nC_6, Ben, and CH), as the pressure increases from 0.2 to 0.8 MPa, their rate constant pressure coefficients are ordered as follows: 3-MP ($\Delta k/\Delta P = 0.20$ MPa^{-1}) > nC_6 (0.15 MPa^{-1}) > Ben (0.13 MPa^{-1}) > CH (0.08 MPa^{-1}) (Fig. 3(b), Table 1).

4. Discussion

4.1. Temperature-pressure controlled light hydrocarbon loss rates

Experimental results demonstrate that elevated temperatures significantly accelerate the loss of LHs. The essence of evaporation is the process by which liquid-phase molecules overcome surface tension and intermolecular forces to escape into the gas phase. The rate constant (K) of this process adheres to the Arrhenius equation (Eq. (2)):

$$K = A \cdot e^{-(E_a/RT)} \quad (2)$$

where E_a represents the activation energy for evaporation, A is the pre-exponential factor, R is the universal gas constant (8.314 J·mol^{-1}·K^{-1}), and T is the absolute temperature (K). This equation indicates that the evaporation rate constant increases exponentially with rising temperature. From a thermodynamic perspective, an increase in temperature enhances the average kinetic energy of liquid-phase molecules, thereby intensifying molecular motion and collision frequency. Concurrently, the saturation vapor pressure of LHs increases considerably, promoting the transfer of molecules from the liquid to the vapor phase (Logan, 1982). The Clausius–Clapeyron equation ($\ln p_{sat} \propto 1/T$) explicitly describes the exponential relationship between saturation vapor pressure and temperature (Rykov et al., 2023). It is

empirically observed that a 10 °C increase in temperature can lead to a several-fold rise in the saturation vapor pressure of LHs. This serves as the fundamental thermodynamic basis for temperature-driven evaporation loss (Rätzsch and Kehlen, 1983).

In open systems, the overall loss rate is often controlled by the mass transfer rate at the gas-liquid interface. The mass transfer coefficient is also positively correlated with temperature. Elevated temperatures reduce liquid viscosity and surface tension while increasing gas-phase diffusivity. These combined physicochemical changes enhance interphase transport efficiency, enabling hydrocarbon vapors to be removed more rapidly from the liquid surface. This continual displacement sustains and amplifies the evaporation process.

Contrary to the effect of temperature, a decrease in pressure enhances the loss rate of LHs. This result might be explained by Henry's Law regarding the solubility of gases in liquids. This law states that, at a constant temperature, the solubility of a gas in a liquid (expressed as a mole fraction) is directly proportional to the gas's partial pressure above the solution (Eq. (3)). In the context of this study, when the total system pressure increases, the partial pressure of LHs also rises, leading to an increase in their solubility in the liquid phase. Experiments have confirmed that pressurization shifts the phase equilibrium towards dissolution. Under low-pressure conditions, the solubility of LHs in the liquid phase decreases, which in turn promotes more molecules to escape into the gas phase.

$$H = P/x \tag{3}$$

where H is Henry's constant, x is the mole fraction of the volatile solute in the solution, and P is the partial pressure of the volatile solute at equilibrium above the liquid.

4.2. Variation of light hydrocarbon parameters with temperature and pressure

4.2.1. Parameters related to source type and depositional environments

Mango (1987) proposed a steady-state catalytic kinetics causality model. Based on the generation kinetic characteristics of C_7 isomers, including 2-methylheptane (2-MH), 3-methylheptane (3-MH), 2,3-dimethylpentane (2,3-DMP), and 2,4-dimethylpentane (2,4-DMP), he established two key parameter ratios: K_1=(2-MH+2,3-DMP)/(3-MH+2,4-DMP) and K_2 = P3/(P2 + N2), where P2 = 2-MH + 3-MH, P3 = 2,2-DMP + 2,4-DMP + 3,3-DMP, and N2 = 1,1-dimethylcyclopentane (DMCP) + 1,3-DMCP (*cis* + *trans*). Studies have shown that K_1 and K_2 values differ significantly among oils of different origins. In this study, the K_1 value of the samples remained stable around 1.06 throughout the experiments (Fig. 4), even when the experimental conditions changed significantly (temperature increased from 35 to 80 °C, and pressure increased from 0.2 to 0.8 MPa). The maximum relative change in K_1, calculated as 100% × (experimental value−initial value)/initial value, was only 5%, indicating high stability of this parameter. In contrast, the K_2 value exhibited greater sensitivity to evaporation and gas washing processes. It decreased from an initial value of 0.14 to 0.06, corresponding to a relative change of 50% (Fig. 4). This difference may be attributed to the following mechanisms: Firstly, the compounds 3-MH and 2,4-DMP, as well as 2-MH and 2,3-DMP, achieved dynamic compensation through differing evaporation rates. Methylhexanes were relatively less affected in the early stages of evaporation, whereas dimethylpentanes experienced significant concentration changes even during short-term evaporation. This disparity in evaporation behavior resulted in a complementary effect between these compounds. Additionally, the K_2 parameter includes the N2 (dimethylcyclopentane) component, with 1,1-DMCP being the most volatile. This compound was completely lost in the early stages of the experiment, further amplifying the observed changes in K_2 values. These findings are consistent with those reported in previous studies. In particular, Cañipa-Morales et al. (2003) demonstrated that the K_1 parameter remains stable for discriminating homologous oils, as it continues to effectively indicate reservoir source identity even in cases of partial evaporation, suggesting a relatively minor influence of evaporative effects on this metric.

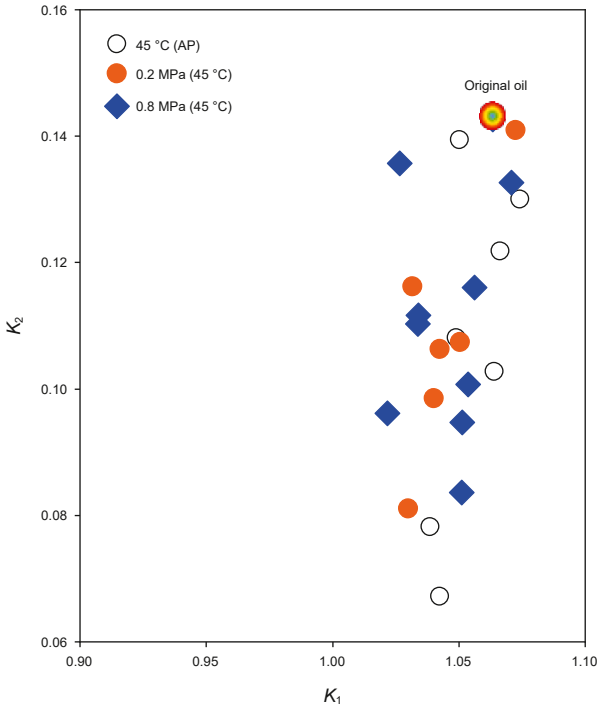

Fig. 4. Variations in K_1 and K_2 under different experimental conditions. (AP: ambient pressure).

Oil-oil correlation is a crucial aspect of petroleum geochemical research, and the star diagram analysis based on LH composition has been widely applied due to its intuitiveness and effectiveness (Lerch et al., 2016; Wever, 2000). Among these methods, the C_7 oil correlation star diagram (C_7-OCSD) established by Halpern (1995) has proven to be an effective tool for identifying the homogeneity of crude oils. The core principle is that oil from the same source exhibits highly similar contour characteristics on star plots. In this study, light oil samples treated under different temperature and pressure conditions were analyzed using the Halpern diagram. The results showed that compared with the original samples, the star diagram parameters of the light oils treated under temperature and pressure conditions underwent systematic changes: the values of the C1 and C3 parameters significantly decreased, while the C2, C4, and C5 parameters increased markedly (Fig. 5). Further analysis of the data indicates that under the same gas washing duration, an increase in temperature accelerates the rate of parameter change, whereas an increase in pressure decelerates it. Taking the 4-h experiment as an example, under 0.2 MPa and at 45 °C, the value of parameter C2 increased from 0.8 to 1.0, with a rate of change of 0.05/h. At 80 °C, it increased from 0.8 to 1.1, with a rate of change of 0.08/h. In contrast, under 0.8 MPa and at 45 °C, the value of C2 increased by only 0.02, with a rate of change of 0.004/h, which is significantly lower than that under 0.2 MPa (0.05/h). This parameter differentiation clearly reveals that

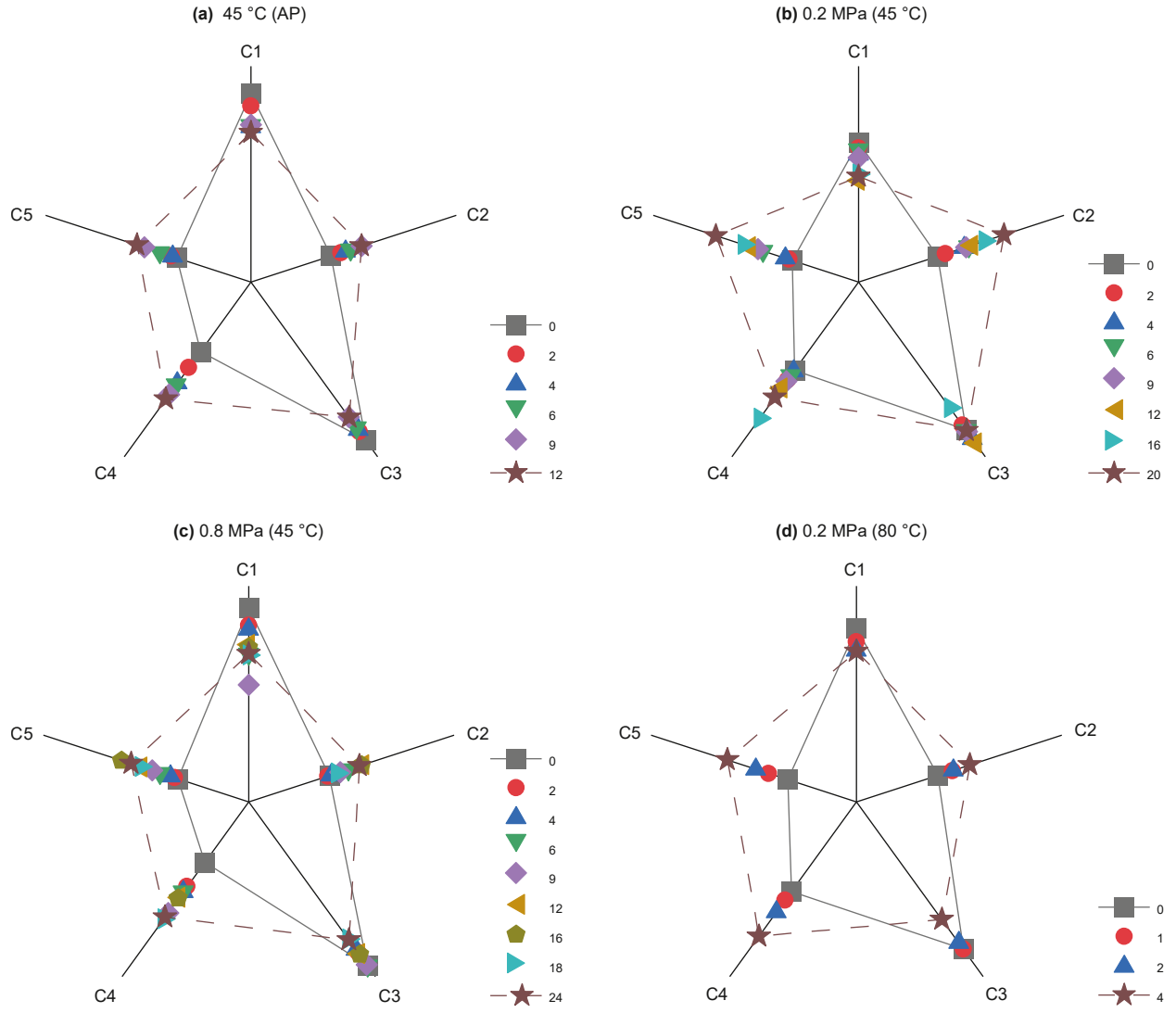

Fig. 5. Variations in the C_7-OCSD star diagram under different experimental conditions. (P3 = 2,2-DMP + 2,4-DMP + 3,3-DMP, C1 = 2,2-DMP/P3, C2 = 2,3-DMP/P3, C3 = 2,4-DMP/P3, C4 = 3,3-DMP/P3, C5 = 3-EP/P3.)

different LH compounds constituting the star diagram have significantly different sensitivities to secondary alteration processes (such as evaporation fractionation and gas washing). The original oil samples typically exhibited a distinct C1–C3 dominant distribution on the star diagram. However, after experimental treatment, the star diagram morphology of the samples underwent a fundamental transformation, presenting a more balanced five-wing symmetric distribution pattern. The significant differences in the star diagram morphology between the original and treated samples strongly confirm that evaporation fractionation (Cañipa-Morales et al., 2003) and gas washing have a strong modifying effect on the LH composition, especially on the key parameters selected for the star diagram.

The ternary diagram based on C_7 LHs—specifically, the relative contents of methylcyclohexane (MCH), the sum of dimethylcyclopentanes (ΣDMCP), and *n*-heptane (nC_7)—is widely used to infer the type (e.g., sapropelic vs. humic) and sedimentary environment (e.g., marine or lacustrine) of the source organic matter associated with oils (Hu et al., 2014; Liu et al., 2015; Wever, 2000). The biological foundations of this method are well established. MCH primarily stems from the thermal transformation of terrestrial organic matter, including compounds such as lignin, cellulose, and alcohols derived from higher plants. Its molecular structure imparts significant thermodynamic stability. As a result, elevated levels of MCH in oil generally signify a substantial contribution of terrestrial organic matter to the source rock. DMCPs predominantly inherit their cyclic structure from lipids associated with aquatic organisms, such as algae and plankton, and are widely recognized as characteristic indicators of sapropelic organic matter input and the corresponding petroleum (Han et al., 2017). nC_7 mainly originates from straight-chain biogenic precursors found in algae and bacteria (Chung et al., 1998). An elevated abundance of nC_7 typically reflects a significant proportion of sapropelic (lipid-rich) organic matter within the source rock (Leythaeuser et al., 1979).

The projection of the original sample on the C_7 LH ternary diagram clearly falls within the typical region of lacustrine humic oil, which is highly consistent with the conclusion drawn by Wang et al., 2024 that the oil in this region is of lacustrine humic origin, based on geochemical evidence. The key finding is that even after experiencing secondary alteration processes (simulating evaporation fractionation and gas washing) of varying durations and intensities (temperature and pressure), all altered samples' projection points on the ternary diagram remain within the

lacustrine humic region defined by the original sample (Fig. 6). Notably, regardless of whether the samples were treated under different temperatures (Fig. 6(a)) or different pressures (Fig. 6(b)), their projection points are highly clustered around the original sample point, without any systematic offset trend. This high consistency of results under various alteration conditions strongly indicates that changes in temperature and pressure during evaporation fractionation and gas washing have extremely limited. This finding has significant practical implications, as it confirms that the C_7 ternary diagram method can reliably and stably indicate the original source type and sedimentary facies information of oil samples subjected to secondary alterations (particularly evaporative fractionation and gas washing). This significantly enhances the method's applicability and credibility in oil-source correlation and depositional environment identification within complex reservoirs affected by secondary alteration processes.

4.2.2. Parameters related to maturity

The cross-plot of the ratios MCH/(MCH + nC_7) and Tol/(Tol + MCH) has been demonstrated to be an effective tool for determining the thermal maturity of oil (Zhang et al., 2020). With progressive thermal maturation, the relative concentration of nC_7 exhibits a marked increase. In contrast, MCH, as a typical cycloalkane, undergoes progressive ring-opening reactions at elevated temperatures, yielding either linear alkanes or aromatic compounds (Brown and King, 1989; Lobo-Lapidus et al., 2008). This transformation results in a negative correlation between the value of MCH/(MCH + nC_7) and thermal maturity. On characteristic cross-plots, the maturation pathway is clearly reflected in systematic variations in molecular ratios: samples evolve from domains characterized by high MCH/(MCH + nC_7) and low Tol/(Tol + MCH) values toward regions exhibiting the inverse relationship (Fig. 7(a)). This consistent trend effectively illustrates the progressive molecular transition from cycloalkane-dominated to aromatic-enriched hydrocarbon assemblages during thermal maturation. Notably, an opposite evolutionary trend was observed under specific physicochemical conditions in this study. With increasing evaporation and gas washing, the directions of change for both MCH/(MCH + nC_7) and Tol/(Tol + MCH) ratios were the same, with both ratios increasing (Fig. 7(a)). Further controlled experiments revealed the effects of temperature and pressure on the slope of the evolutionary trajectory: under constant pressure (atmospheric pressure), when the temperature increased from 35 to 80 °C, the slope of the linear evolutionary trajectory connecting the two ratios increased significantly from 0.8 to 2.0 (Fig. 7(b)). This indicates that an increase in temperature amplified the growth of the MCH/(MCH + nC_7) ratio while relatively weakening the growth of the Tol/(Tol + MCH) ratio. Under constant pressure (0.2 MPa), heating from 45 °C to 80 °C also resulted in a significant increase in the slope of the evolutionary trajectory (Fig. 7(c)). However, constant temperature conditions (45 °C), an increase in pressure (Fig. 7(d)) led to a slight decrease in the slope of the evolutionary trajectory, suggesting that an increase in pressure may more significantly promote the increase in the Tol/(Tol + MCH) ratio. Compared to the evaporation process at atmospheric pressure (~0.1 MPa) and 45 °C (which exhibits an evolutionary trajectory slope of 1.1) (Fig. 7(b)), the rate of change in the MCH/(MCH + nC_7) ratio increases to a slope of 1.2 during gas washing under slightly elevated pressure (0.2 MPa). However, when pressure increases beyond a certain threshold (e.g., 0.8 MPa), its inhibitory effect becomes dominant, reducing the corresponding slope to 1.0. This phenomenon indicates the existence of a critical pressure threshold governing the impact of pressure on LH fractionation. Below this threshold, increasing pressure may enhance molecular fractionation, potentially by increasing gas solubility in the oil phase or altering vapor-liquid equilibrium. Conversely, above this threshold, high-pressure conditions tend to suppress selective molecular migration, leading to diminished or even stagnant fractionation effects.

In summary, the cross plot of MCH/(MCH + nC_7) versus Tol/(Tol + MCH) serves as a classical indicator of thermal maturity, whose geochemical significance is established in high-temperature thermal evolution processes. However, this study demonstrates that even under low-temperature conditions, secondary phase fractionation processes (such as evaporative fractionation and gas washing), as physical partitioning mechanisms, can significantly alter the distribution of these ratios and induce evolutionary patterns contrary to or more complex than those driven solely by thermal maturation.

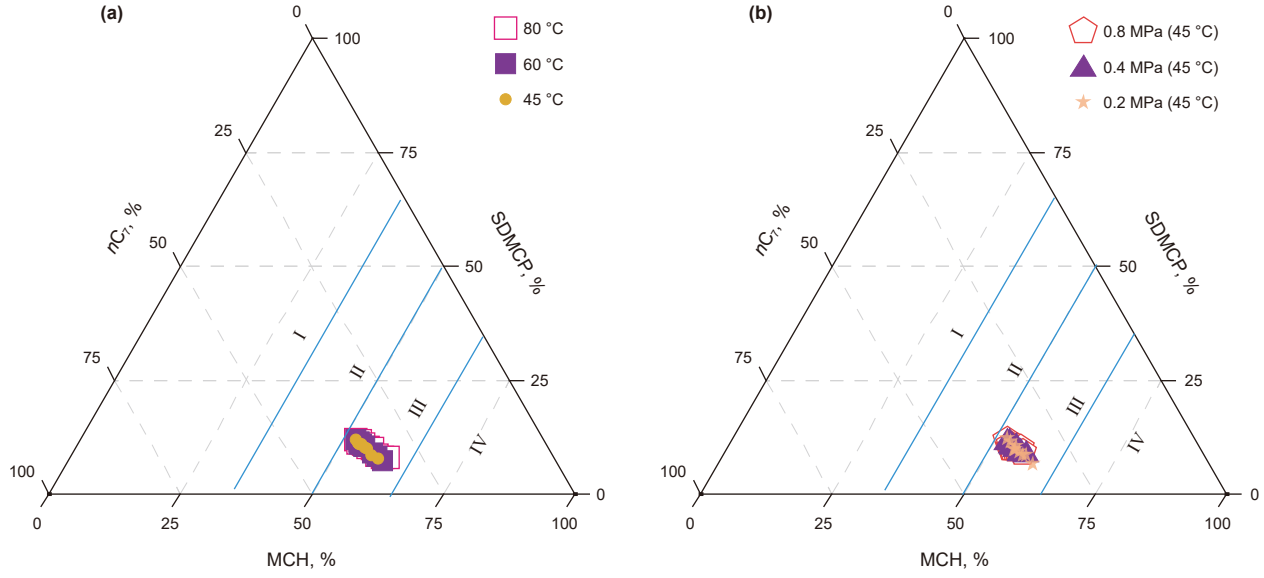

Fig. 6. MCH-ΣDMCP-nC_7 ternary diagram under atmospheric pressure **(a)** and constant temperature **(b)** experimental conditions (the source type plate is from Hu et al. (1990) and Deng et al. (2023), I: marine sapropel, II: lacustrine sapropel, III: lacustrine humic, IV: coal-derived oil).

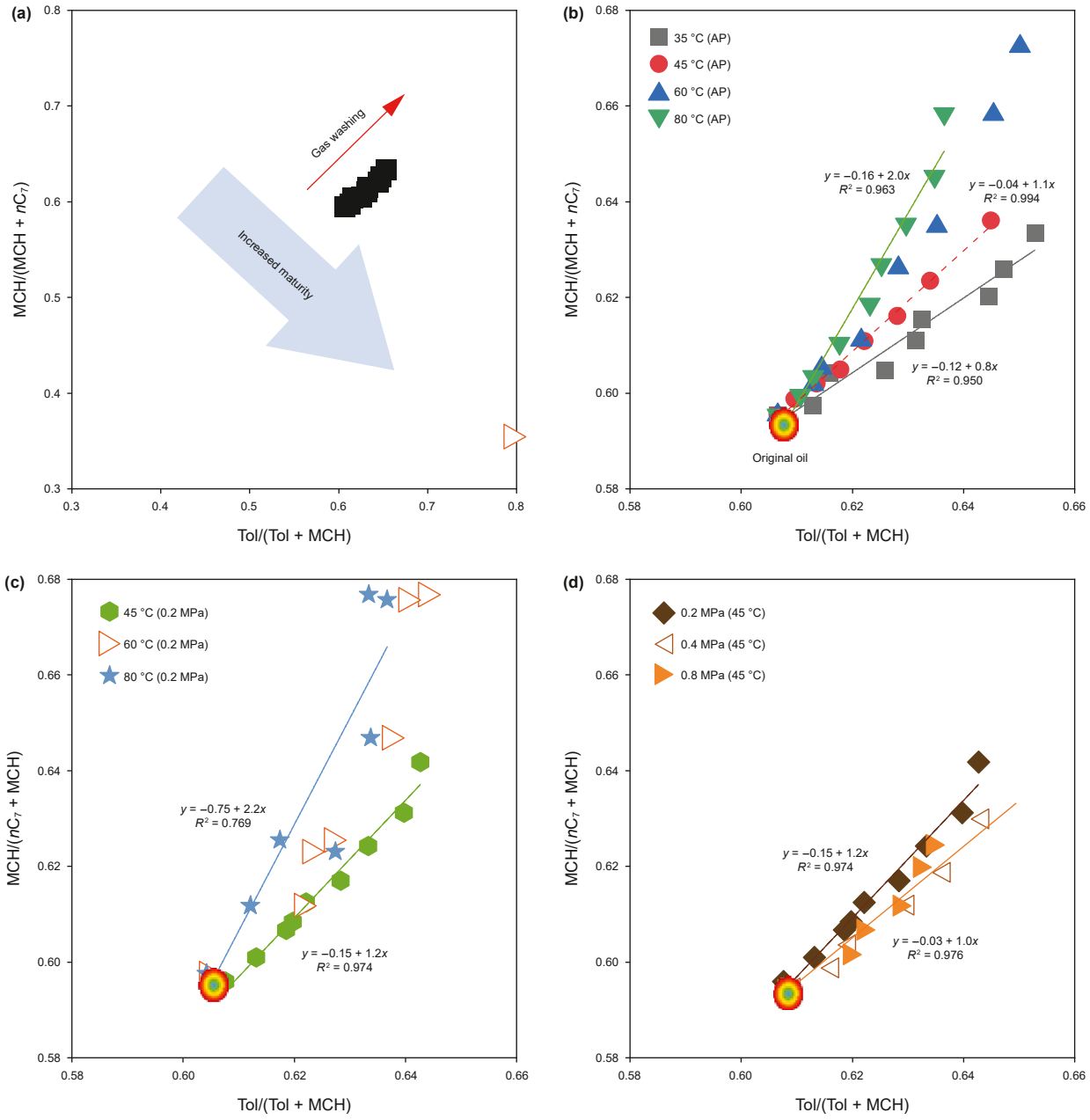

Fig. 7. Ratios of MCH/(MCH + nC_7) and Tol/(Tol + MCH) under different experimental conditions.

The ratio of 2,4-dimethylpentane (2,4-DMP) to 2,3-dimethylpentane (2,3-DMP) serves as a temperature-sensitive indicator, thus reflecting the thermal maturity of genetically related oils (Hu et al., 1990; Mango, 1987). The calculation formula is Ctemp (°C) = 140 + 15 × ln (2,4DMP/2,3DMP) (BeMent et al., 1994). The ratio depends on the generation temperature and is influenced by heating rates or the source of organic matter (Mango, 1997). This study reveals the high sensitivity of this temperature indicator to secondary alteration processes. The original samples, which were not experimentally treated, yielded an inferred oil expulsion temperature of 132.0 °C (Fig. 8), while the experimentally treated samples showed calculated temperatures that decreased to 113.0 °C (Fig. 8(b)), with a maximum reduction of 19 °C. This significant systematic underestimation of temperature is primarily attributed to systematic shifts in the ratio of 2,4-DMP to 2,3-DMP during vapor-liquid partitioning processes (e.g., evaporative fractionation or gas washing), resulting from their inherent volatility disparity. This finding corroborates previous experimental observations. Cañipa-Morales et al. (2003) demonstrated in isothermal evaporation experiments at 20 °C that the DMP thermometer-derived estimates for processed oil samples could be reduced by 5–15 °C compared to the original sample as evaporation progressed. The inhibitory effect of pressure on fractionation behavior, as discussed above, is further corroborated by changes in the LH maturity parameter, Ctemp (°C). Through linear regression of Ctemp (°C) against time, this study reveals the critical influence of pressure variation on the fractionation rate: Under evaporation conditions at atmospheric pressure (~0.1 MPa) and 45 °C, the rate of Ctemp (°C) change is 0.59 °C/h (Fig. 8(a)). During gas washing at the same temperature (45 °C) but under slightly elevated pressure (0.2 MPa), this rate increases slightly to 0.79 °C/h (Fig. 8(b)). However, when pressure is further increased to 0.8 MPa,

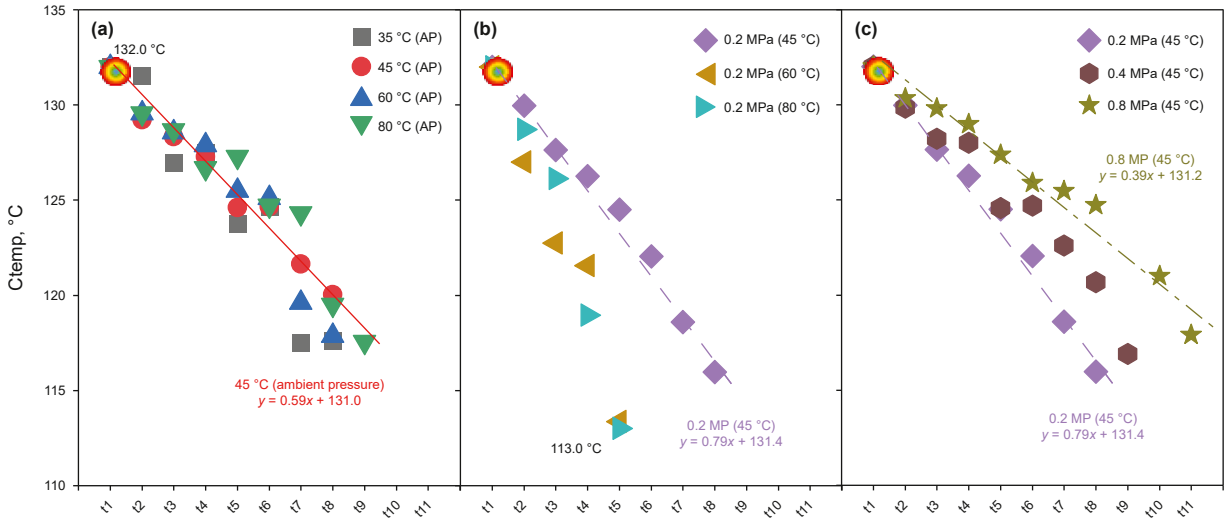

Fig. 8. Plot of calculated temperature (Ctemp) of residual oil during the experiment.

the rate of Ctemp change decreases significantly to 0.39 °C/h (Fig. 8(c)). This attenuation in rate clearly confirms the suppression of LH fractionation under high-pressure conditions. These findings hold significant implications for utilizing LH parameters to estimate geological temperatures. As previously noted, in geological environments reaching a certain pressure threshold (e.g., tens of MPa), the "preservation effect" of high pressure would significantly inhibit or essentially halt fractionation processes. Consequently, parameters resistant to such secondary alteration may prove reliable indicators for estimating petroleum expulsion temperatures under geological conditions.

Traditional DMP thermometer models are based on a critical assumption: hydrocarbon generation and evolution take place in relatively closed thermodynamic systems. However, actual geological processes in petroleum reservoirs (e.g., migration, accumulation, and particularly phase fractionation within the reservoir) often operate under open or semi-open system conditions. This study, in conjunction with prior work, demonstrates that phase fractionation processes (e.g., evaporative fractionation, gas washing) in open systems can significantly alter the original compositional characteristics of LHs, especially the relative proportions of isomers with differing volatilities. This alteration leads to deviations in temperature inversion results based on the 2,4-DMP/2,3-DMP ratio from the true hydrocarbon generation temperature. Therefore, when utilizing LH parameters (such as DMP isomer ratios) to reconstruct basin thermal history or source rock expulsion temperatures, it is imperative to recognize the potentially substantial superimposed influence of secondary alteration processes within the reservoir—particularly phase fractionation—on LH signatures. A holistic assessment of these secondary effects is crucial for accurately interpreting the temperature signal and avoiding misleading interpretations of thermal maturity history.

4.2.3. Parameters related to secondary alteration

The distribution patterns of monocyclic aromatic hydrocarbons (e.g., benzene and toluene) in petroleum systems are governed by the interplay between primary geochemical controls and secondary alteration processes. Regarding primary factors, the type of original organic matter is key to determining their initial abundance. Terrestrial higher plant-derived organic matter, characterized by lignin and cellulose inputs, undergoes pronounced demethylation and aromatization during thermal maturation, yielding substantially enriched aromatic compounds (Leythaeuser et al., 1979). Consequently, such systems exhibit markedly higher aromatic-to-alkane ratios compared to lacustrine shale systems dominated by aquatic organic matter. Regarding secondary processes, post-generation physical fractionation mechanisms profoundly modify original hydrocarbon compositions. Phase separation phenomena during migration or reservoir emplacement (e.g., gas washing and evaporative fractionation) preferentially deplete volatile components, resulting in relative enrichment of monocyclic aromatic hydrocarbons (Thompson, 1987). Application of Thompson's (1987) paraffinicity-aromaticity framework to our experimental oils reveals substantial compositional deviations attributable to these fractionation processes (Fig. 9(a)), reflecting the differential volatility between Tol, MCH, and nC_7.

Series I: With prolonged evaporation time under atmospheric pressure, the Tol/nC_7 value in the residual light oil systematically increased from 2.27 to 3.17–3.82, reflecting enrichment of the aromatic compound (Tol) relative to the *n*-alkane (nC_7). Concurrently, the nC_7/MCH value decreased systematically from 0.68 to 0.49–0.57, indicating depletion of *n*-alkanes relative to the cycloalkanes (methylcyclohexane) (Fig. 9(b)). A strong negative correlation ($R^2 > 0.9$) was observed between Tol/nC_7 and nC_7/MCH. These trends align with Thompson's (1987) evaporative fractionation kinetic model, confirming the effectiveness of these ratios as sensitive indicators of phase fractionation (Fig. 9(a)). Elevated temperatures partially suppressed the magnitude of increase in Tol/nC_7 while amplifying the decrease in nC_7/MCH. As temperature rose from 35 °C to 80 °C, the slope of the linear increase rate in Tol/nC_7 declined from 9.6 to 6.9 (Fig. 9(b)), suggesting that heating inhibits aromatic-alkane fractionation. Conversely, the rate of decrease in nC_7/MCH accelerated correspondingly (Fig. 9(b)). This divergence arises because heating reduces liquid viscosity, enhancing the evaporation of lighter components like nC_7. However, high-boiling-point aromatics (Tol bp = 110.6 °C) are less affected by temperature than medium-boiling-point cycloalkanes (MCH bp = 100.9 °C), leading to differentiated fractionation behavior.

Series II: Under constant pressure, gas washing produced residual oil LH trends similar to Series I experiments: Tol/nC_7 increased to 3.22–6.10 (exceeding the maximum of Series I: 3.82), while nC_7/MCH decreased to 0.38–0.27 (below the minimum of Series I: 0.49). Pressure significantly attenuated the regulatory

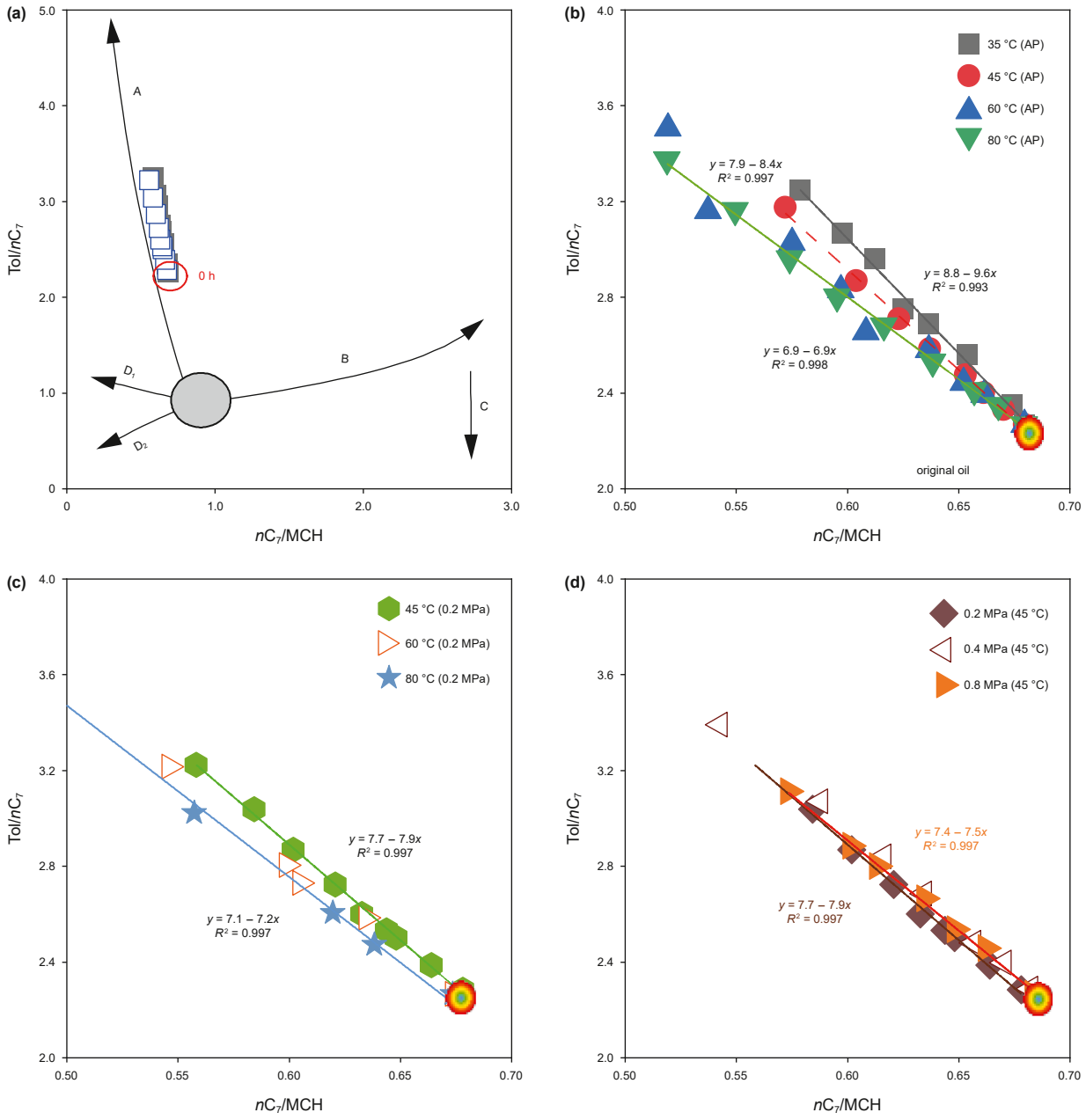

Fig. 9. Correlation plots of Tol/nC_7 and nC_7/MCH values under different experimental conditions (diagram modified after Thompson (1987)). (A: Evaporation fractionation; B: Maturation; C: Water washing; D: Biodegradation.)

impact of temperature on fractionation: when temperature increased from 45 °C to 80 °C, the rate of increase in Tol/nC_7 only declined slightly from 7.9 to 7.2 (a reduction of 8.9%, markedly lower than the 28% decrease observed under atmospheric conditions, Fig. 9(c)).

Series III: The residual oil exhibited an evolutionary trend similar to that of the isothermal evaporation experiments: the Tol/nC_7 ratio increased from 2.27 to 3.0–3.4, and the nC_7/MCH ratio decreased from 0.68 to 0.54–0.57. As the experimental pressure increased from 0.2 MPa to 0.8 MPa (Fig. 9(d)), the slope of the line formed by the Tol/nC_7 and nC_7/MCH ratios decreased slightly from 7.9 to 7.5. The small magnitude of this change suggests that the influence of pressure on fractionation behavior is relatively limited within this low-pressure range.

The observed reduction in the variation of Tol/nC_7 ratios with increasing pressure suggests that diffusive transport is already being suppressed within the experimental pressure window. Although the maximum pressure applied here falls far short of realistic reservoir conditions, the directional trend aligns with mechanisms identified through molecular simulation. For example, molecular dynamics simulations of shale nanoporous systems demonstrate that elevated pressure markedly reorganizes the spatial distribution and diffusion kinetics of hydrocarbon molecules. Under high pressure, lighter hydrocarbons are preferentially expelled toward mineral surfaces, while their diffusion coefficients decrease nonlinearly (Ren et al., 2025). In recent years, molecular dynamics simulations have emerged as a powerful tool for probing the behavior of light hydrocarbons in confined pores under high pressure, offering a reliable bridge for extrapolating low-pressure experimental trends. Ren et al. (2025), in their simulation of multicomponent hydrocarbons within kerogen–illite composite pores, reported that increasing pressure from 11 to

35 MPa drove a progressive migration of light hydrocarbons from organic matter surfaces toward clay mineral interfaces, accompanied by significantly hindered diffusion. This trend is mechanistically consistent with the attenuation of fractionation observed in our study as pressure rises, further supporting the inference that light hydrocarbon mobility declines and fractionation may approach stagnation under high-pressure reservoir conditions. Molecular responses, including diffusive capacity, represent continuous functions of pressure and temperature; thus, trends discerned at low pressure are expected to be accentuated under more extreme conditions (Gautam et al., 2019; Parage et al., 2024). According to the Stokes–Einstein relation and high-pressure fluid theory, the diffusion coefficient generally decreases exponentially with increasing pressure. Due to the more flexible molecular structure and higher compressibility of n-alkanes (such as nC_7) under high pressure compared to aromatic compounds (such as Tol), their diffusion capacity is likely to be inhibited more strongly. Therefore, we infer that under high geological pressures of tens of MPa, the variation in the Tol/nC_7 ratio is expected to be significantly enhanced, as the relative migration efficiency of nC_7 decreases more markedly.

On the other hand, the behavior of the nC_7/MCH ratio differs. As a cycloalkane, methylcyclohexane (MCH) possesses a relatively rigid molecular structure, and the mechanism by which pressure influences its diffusion differs from that of *n*-alkanes. In shallow or normal-pressure reservoirs, the fractionation effect of gas washing (such as the decrease in nC_7/MCH) is primarily controlled by differences in the solubility of hydrocarbon components in the gas. However, as pressure increases to geological conditions of tens of MPa, molecular diffusion is significantly suppressed, leading to a general decline in the efficiency of oil and gas mass transfer (Chen et al., 2019; Thompson, 1987). Under such circumstances, the selective extraction mechanism based on solubility differences may become ineffective due to restricted molecular movement, ultimately causing changes in ratios such as nC_7/MCH to tend toward stagnation.

Thus, although the slope change observed in the current low-pressure experiments is subtle, it provides important clues for understanding fractionation behavior under higher pressures. Future work should prioritize conducting simulation experiments under higher-pressure conditions to quantitatively characterize the response of Tol/nC_7 and nC_7/MCH ratios, thereby enabling more accurate assessment of hydrocarbon composition behavior in deep reservoirs and the applicability of maturity evaluation indicators.

4.3. Quantitative evaluation of gas washing

The logarithm of the molar concentration of *n*-alkanes in crude oil that has not undergone any fractionation or alteration exhibits a linear relationship with the carbon number (Kissin, 1987), which can be expressed as:

$$\lg[\mathrm{MC}(n)] = a \cdot n + \lg(\mathrm{A}) \tag{4}$$

Here, MC(n) represents the mass molar concentration of *n*-alkanes (the ratio of the mass percent concentration of normal alkanes in crude oil to their molecular weight), n is the carbon number of the *n*-alkane, A is a normalization factor, and a is the distribution slope parameter. Crude oil subjected to gas washing will experience systematic shifts in the distribution characteristics of *n*-alkanes. High-carbon-number *n*-alkanes (C_{20+}) typically remain unaffected by gas-phase extraction due to their low volatility and solubility, and their distribution continues to follow the linear law described by Eq. (4). However, low-carbon-number *n*-alkanes (C_{10}–C_{18}) preferentially dissolve in the invading gas phase (e.g., methane) and are removed, resulting in a significant decrease in their concentration in the residual oil phase. This selective

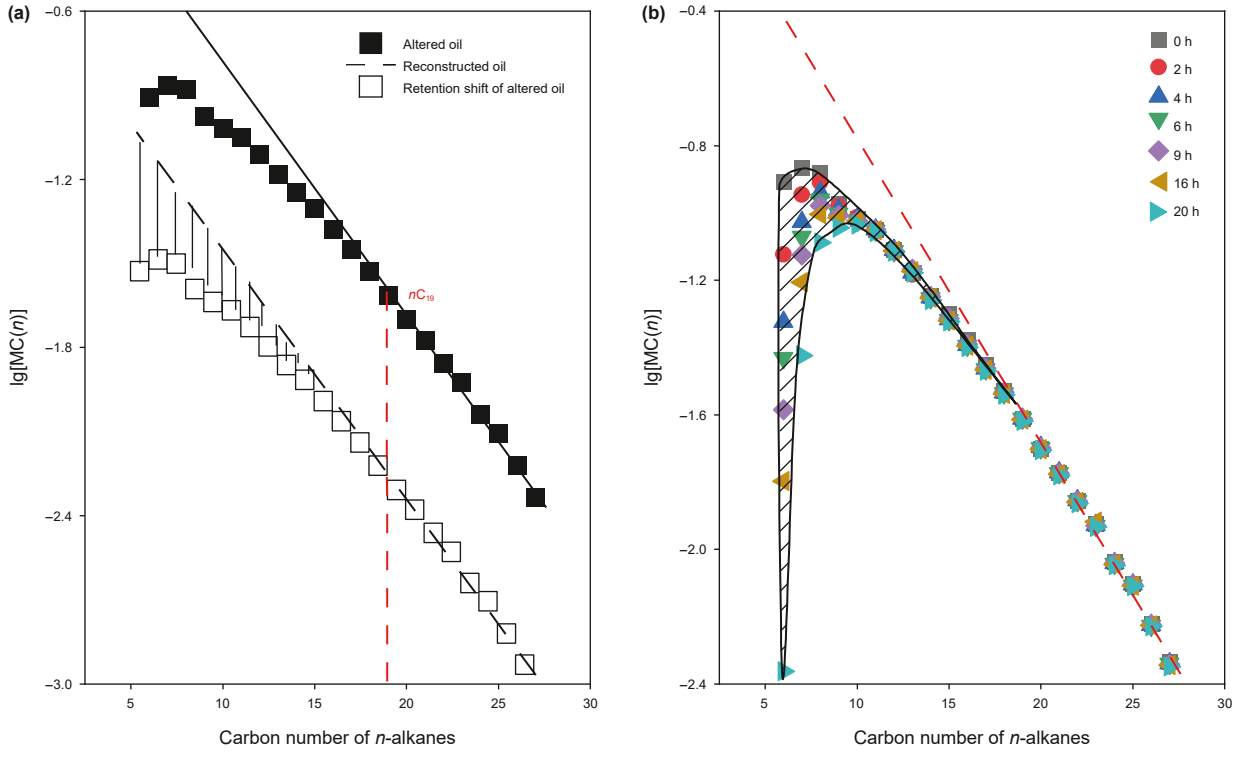

Fig. 10. (**a**) Schematic diagram of the calculation method for *n*-alkane loss rate in untreated samples, (**b**) the calculation of *n*-alkane loss rate under different methane gas washing durations at 0.2 MPa (45 °C) conditions in this study.

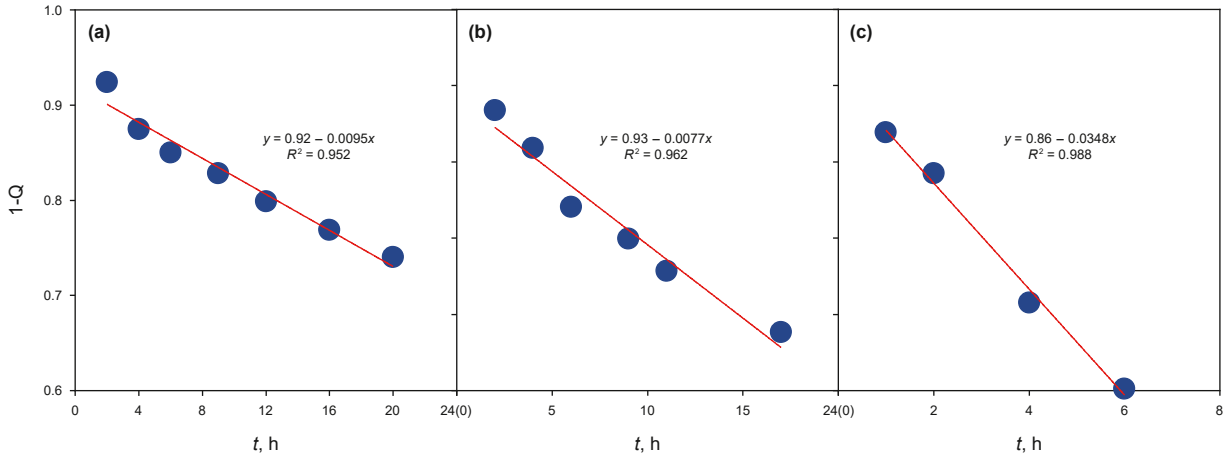

Fig. 11. Relationship between the remaining mass percentage of *n*-alkanes and gas washing time ((**a**), (**b**), and (**c**) correspond to experimental conditions of 0.2 MPa (45 °C), 0.4 MPa (45 °C), and 0.2 MPa (80 °C), respectively).

removal disrupts the original linear relationship, primarily manifested as deviations of data points in the low-carbon-number range from the regression line determined by the high-carbon-number range (Fig. 10(a)). In crude oil affected by gas washing, high-carbon-number *n*-alkanes remain essentially unaffected, while low-carbon-number *n*-alkanes are dissolved and carried away by the gas phase, causing a deviation from the linear relationship described by Eq. (4). By establishing a linear regression equation for the high-carbon-number range, the original distribution of low-carbon-number *n*-alkanes before gas washing can be reconstructed, thereby quantitatively assessing the intensity of gas washing effects (Fig. 10(a)). Based on this principle, this study quantitatively calculated the loss of each carbon-number alkane and the overall gas washing intensity by comparing the measured concentrations in the original oil samples and the residual oil after gas washing. The results of continuous methane gas washing experiments provided strong validation for the above model and revealed a significant time effect. With increasing gas washing time, the molar concentration of low-carbon-number normal alkanes (C_{10}–C_{18}) in the residual light oil systematically decreased. The shaded areas in Fig. 9(b) intuitively quantify the cumulative loss of each carbon-number alkane component over different gas washing periods. Crucially, the high-carbon-number range (C_{20+}) maintained an excellent linear distribution throughout the entire gas washing process (Fig. 10(b)), which is fully consistent with the assumptions of the Kissin model and strongly confirms the reliability of the model and its inversion algorithm in studying gas washing effects.

Furthermore, this study quantitatively evaluated the effects of temperature and pressure conditions on gas washing efficiency. Experiments revealed that light oil samples treated under different temperatures (45–80 °C) and pressures (0.2–0.4 MPa) exhibited a significant linear negative correlation between (1-Q) (relative residual mass fraction of *n*-alkanes) and gas washing time (t) (Fig. 11). The absolute value of the slope of this linear relationship ($|k'|$, h^{-1}) quantitatively characterizes the overall loss rate of light components (represented by the sum of *n*-alkanes) within the experimental system. Sensitivity analysis indicated that within the temperature range of 45–80 °C, increasing temperature resulted in an elevated loss rate, with a temperature sensitivity coefficient calculated as $\approx 0.0007\ ^{\circ}C^{-1}$ (i.e., $\Delta|k'|/\Delta T = (0.0348 - 0.0095)/(80 - 45) \approx 0.0007\ ^{\circ}C^{-1}$; see Table 2). Pressure sensitivity was significantly higher: within the range of 0.2 to 0.4 MPa, increasing pressure also led to an increase in the loss rate, with a pressure sensitivity coefficient calculated as $\approx 0.01\ MPa^{-1}$ (i.e., $\Delta|k'|/\Delta P = (0.0077 - 0.095)/(0.4 - 0.2) = 0.009\ MPa^{-1} \approx 0.01\ MPa^{-1}$; see Table 2). Comparison of the sensitivity coefficients demonstrates that a unit pressure change (1 MPa) induces a greater increase in the loss rate than a unit temperature change (1 °C). This clearly indicates that, within the simulated reservoir temperature and pressure conditions, pressure exerts a more dominant control than temperature over gas invasion efficiency (i.e., the loss rate of light components).

Table 2
Quantitative results of gas washing after different experimental durations (*Q* represents the loss compared to untreated samples after a certain processing time).

	*Q*1	*Q*2	*Q*3	*Q*4	*Q*5	*Q*6	*Q*7	*k*'
0.2 MPa (45 °C)	7.6	12.5	15.0	17.1	20.1	23.1	26.0	0.0095
0.4 MPa (45 °C)	10.3	12.3	15.4	17.0	18.7	21.9	22.0	0.0077
0.2 MPa (80 °C)	18.1	20.8	29.3	34.9				0.0348

5. Conclusion

(1) Employing a gas-washing simulation apparatus, this study investigated temperature and pressure effects on light hydrocarbon loss rates. Elevated temperature significantly accelerated light hydrocarbon loss rates, while increased pressure suppressed it. The sensitivity to temperature and pressure variations was determined by carbon number and molecular structure: for similar structures, lower molecular weight compounds exhibited greater sensitivity; for the same carbon numbers, cycloalkanes showed the least temperature and pressure sensitivity.

(2) Among source and depositional environment indicators, Mango parameter K_1 and the C_7 light hydrocarbons ternary diagram remained persistently stable post-gas-washing and were minimally affected by temperature and pressure changes, confirming their reliability for tracing original organic matter sources and depositional environments. In contrast, parameter K_2 and the C_7-OCSD star diagram were significantly altered by phase fractionation, requiring cautious application.

(3) While maturity increase typically yields a negative correlation between MCH/(MCH + nC_7) and Tol/(Tol + MCH), gas washing induced a positive correlation between them. Consequently, gas-washing significantly distorts maturity

assessment using these ratios. Higher temperature amplified the increase in MCH/(MCH + nC_7) while relatively weakening the increase in Tol/(Tol + MCH). The maturity parameter 2,4-DMP/2,3-DMP proved highly sensitive to gas washing; significant overprinting by secondary reservoir processes (especially phase fractionation) must be acknowledged when using it.

(4) A significant negative correlation between Tol/nC_7 and nC_7/MCH ratios in our experiments validated Thompson's Paraffinicity-Aromaticity diagram as an effective indicator of phase fractionation. Elevated temperatures partially suppressed the magnitude of increase in Tol/nC_7 while amplifying the decrease in nC_7/MCH.

CRediT authorship contribution statement

Wen-Na Liu: Writing – original draft, Visualization, Methodology, Formal analysis. **Wang-Lu Jia:** Writing – review & editing, Validation, Supervision, Funding acquisition. **Qiang Wang:** Methodology, Investigation. **Jian Chen:** Writing – review & editing, Validation, Supervision. **Jin-Bu Li:** Writing – review & editing, Validation, Supervision. **Ping-An Peng:** Validation, Supervision, Resources, Conceptualization.

Declaration of competing interest

The authors declare that they have no known competing financial interests or personal relationships that could have appeared to influence the work reported in this paper.

Acknowledgements

This study was financially supported by the National Natural Science Foundation of China (42125304 and 42173057). We gratefully acknowledge the reviewers for their insightful and constructive comments and suggestions, which have significantly enhanced the quality of this manuscript. We also thank Min Li for editorial handling.

Supplementary Information

Supplementary Information to this article can be found online at https://doi.org/10.1016/j.petsci.2026.03.031.

References

ASTM, 2001. Standard practice for full-scale chamber determination of volatile organic emissions from indoor materials/products. D 6670-01. American Society of Testing and Materials, West Conshohocken, PA.

BeMent, W.O., Levey, R.A., Mango, F.D., 1994. The temperature of oil generation as defined with a C_7 chemistry maturity parameter; (2,4-DMP/2,3-DMP ratio). In: Abstract, First Joint AAPG/AMPG Research Conference, "Geological Aspects of Petroleum Systems", 2–6 October 1994, Mexéico City.

Bouchard, D., Hoehener, P., Hunkeler, D., 2008. Carbon isotope fractionation during volatilization of petroleum hydrocarbons and diffusion across a porous medium: a column experiment. Environ. Sci. Technol. 42, 7801–7806. https://doi.org/10.1021/es800391s.

Brown, T.C., King, K.D., 1989. Very low-pressure pyrolysis (VLPP) of methyl- and ethynyl-cyclopentanes and cyclohexanes. Int. J. Chem. Kinet. 21, 251–266. https://doi.org/10.1002/kin.550210405.

Cai, C., Li, H., Li, K., et al., 2022. Thermochemical sulfate reduction in sedimentary basins and beyond: a review. Chem. Geol. 607, 121018. https://doi.org/10.1016/j.chemgeo.2022.121018.

Cai, S.Y., Xiao, Q.L., Cheng, T., et al., 2024. Molecular and stable carbon isotopic compositions of crude oils from Shengbei Sag, Tuha Basin: implications for hydrocarbon sources, migration and mixing. Fuel 371 (Part A), 131877. https://doi.org/10.1016/j.fuel.2024.131877.

Cañipa-Morales, N.K., Galán-Vidal, C.A., Guzmán-Vega, M.A., et al., 2003. Effect of evaporation on C_7 light hydrocarbon parameters. Org. Geochem. 34, 813–826. https://doi.org/10.1016/S0146-6380(03)00002-0.

Chen, C., Wang, Y., Beagle, J.R., et al., 2019. Reconstruction of the evolution of deep fluids in light oil reservoirs in the Central Tarim basin by using PVT simulation and basin modeling. Mar. Petrol. Geol. 107, 116–126. https://doi.org/10.1016/j.marpetgeo.2019.05.009.

Chen, J., Deng, C., Wang, X., et al., 2017. Formation mechanism of condensates, waxy and heavy oils in the southern margin of Junggar basin, NW China. Sci. China Earth Sci. 60, 972–991. https://doi.org/10.1007/s11430-016-9027-3.

Chung, H.M., Walters, C.C., Buck, S., et al., 1998. Mixed signals of the source and thermal maturity for petroleum accumulations from light hydrocarbons: an example of the Beryl field. Org. Geochem. 29, 381–396. https://doi.org/10.1016/S0146-6380(98)00063-1.

Deng, H., Zhang, H., Zhang, Y., et al., 2023. Genetic identification of light oils and condensates using δD indices of C_7 hydrocarbons: a case study in the Tarim basin, NW China. Int. J. Coal Geol. 279, 104372. https://doi.org/10.1016/j.coal.2023.104372.

Gautam, S., Liu, T., Cole, D., 2019. Sorption, structure and dynamics of CO_2 and ethane in silicalite at high pressure: a combined monte carlo and molecular dynamics simulation study. Molecules 24 (1), 99. https://doi.org/10.3390/molecules24010099.

Goldstein, T.P., Aizenshtat, Z., 1994. Thermochemical sulfate reduction a review. J. Therm. Anal. 42, 241–290. https://doi.org/10.1007/BF02547004.

Halpern, H.I., 1995. Development and applications of light-hydrocarbon-based star diagrams1. AAPG (Am. Assoc. Pet. Geol.) Bull. 79, 801–815. https://doi.org/10.1306/8d2b1bb0-171e-11d7-8645000102c1865d.

Han, W., Tao, S., Hu, G., et al., 2017. Light hydrocarbon geochemical characteristics and their application in upper Paleozoic, Shenmu gas field, Ordos basin. Energy Explor. Exploit. 35. https://doi.org/10.1177/0144598716679962.

Hu, G., Yu, C., Tian, X., 2014. The origin of abnormally high benzene in light hydrocarbons associated with the gas from the Kuqa depression in the Tarim Basin, China. Org. Geochem. 74, 98–105. https://doi.org/10.1016/j.orggeochem.2014.01.011.

Hu, T., Ge, B., Chang, Y., et al., 1990. The development and application of fingerprint parameters for hydrocarbons absorbed by source rocks and light hydrocarbons in natural gas. Petrol. Explor. Dev. 4, 375–394. https://doi.org/10.11781/sysydz199004375 (in Chinese).

Huang, Y., Liao, Y., Xu, T., et al., 2023. Characteristics of light hydrocarbons under the superimposed influence of biodegradation and subsequent thermal maturation. Org. Geochem. 177, 104557. https://doi.org/10.1016/j.orggeochem.2023.104557.

Kissin, Y.V., 1987. Catagenesis and composition of petroleum: origin of *n*-alkanes and isoalkanes in petroleum crudes. Geochem. Cosmochim. Acta 51, 2445–2457. https://doi.org/10.1016/0016-7037(87)90296-1.

Lerch, B., Karlsen, D.A., Abay, T.B., et al., 2016. Regional petroleum alteration trends in Barents Sea oils and condensates as a clue to migration regimes and processes. AAPG (Am. Assoc. Pet. Geol.) Bull. 100, 165–190. https://doi.org/10.1306/08101514152.

Leythaeuser, D., Schaefer, R.G., Cornford, C., et al., 1979. Generation and migration of light hydrocarbons (C_2-C_7) in sedimentary basins. Org. Geochem. 1, 191–204. https://doi.org/10.1016/0146-6380(79)90022-6.

Li, B., Pan, Z., He, D., et al., 2025. Fractionation of chain alkanes and its geological significance in PVT gas invasion experiment. Fault-Block Oil Gas Field 32, 126–132. https://doi.org/10.6056/dkyqt202501016.

Liang, B., Balasubramanian, S., Wang, B., et al., 2010. PVT characterisation and compositional modelling of gas condensate and volatile oil reservoirs. Int. J. Oil Gas Coal Technol. 4, 79–102. https://doi.org/10.1504/IJOGCT.2011.037746.

Liu, D., Yu, C., Huang, S., et al., 2015. Using light hydrocarbons to identify the depositional environment of source rocks in the Ordos Basin, central China. Energy Explor. Exploit. 33, 869–890. https://doi.org/10.1260/0144-5987.33.6.869.

Liu, W., Jia, W., Wang, Q., et al., 2024. Influencing factors of hydrogen isotopic fractionation of light hydrocarbons during evaporation and implications. Org. Geochem. 198, 104894. https://doi.org/10.1016/j.orggeochem.2024.104894.

Lobo-Lapidus, R.J., McCall, M.J., Lanuza, M., et al., 2008. Alumina-supported trirhenium clusters: stable high-temperature catalysts for methylcyclohexane conversion. J. Phys. Chem. C 112, 3383–3391. https://doi.org/10.1021/jp709957t.

Logan, S.R., 1982. The origin and status of the Arrhenius equation. J. Chem. Educ. 59, 279. https://doi.org/10.1021/ed059p279.

Losh, S., Cathles, L., Meulbroek, P., 2002. Gas washing of oil along a regional transect, offshore Louisiana. Org. Geochem. 33, 655–663. https://doi.org/10.1016/S0146-6380(02)00025-6.

Machel, H.G., 2001. Bacterial and thermochemical sulfate reduction in diagenetic settings — old and new insights. Sediment. Geol. 140, 143–175. https://doi.org/10.1016/S0037-0738(00)00176-7.

Mango, F.D., 1987. An invariance in the isoheptanes of petroleum. Science 237, 514–517. https://doi.org/10.1126/science.237.4814.514.

Mango, F.D., 1997. The light hydrocarbons in petroleum: a critical review. Org. Geochem. 26, 417–440. https://doi.org/10.1016/S0146-6380(97)00031-4.

Mango, F.D., 2000. The origin of light hydrocarbons. Geochem. Cosmochim. Acta 64, 1265–1277. https://doi.org/10.1016/S0016-7037(99)00389-0.

Parage, B., Miqueu, C., Pérez-Rodríguez, M., et al., 2024. Upper storage-capacity limit and multiple occupancy phenomena in H_2-hydroquinone clathrates

using Monte Carlo and DFT simulations. Phys. Chem. Chem. Phys. 26, 6939–6948. https://doi.org/10.1039/d3cp05331h.
Philippi, G.T., 1975. The deep subsurface temperature controlled origin of the gaseous and gasoline-range hydrocarbons of petroleum. Geochem. Cosmochim. Acta 39, 1353–1373. https://doi.org/10.1016/0016-7037(75)90115-5.
Rabbani, A.R., Asemani, M., Kazemi, H., et al., 2023. Application of light hydrocarbons for classification and geochemistry characterization of condensates from the Gavbendi high, southwest Iran. Mar. Petrol. Geol. 153, 106255. https://doi.org/10.1016/j.marpetgeo.2023.106255.
Rätzsch, M.T., Kehlen, H., 1983. Continuous thermodynamics of complex mixtures. Fluid Phase Equilib. 14, 225–234. https://doi.org/10.1016/0378-3812(83)80129-0.
Ren, W., Zeng, X., Wang, G., et al., 2025. Molecular simulations of a multicomponent hydrocarbon-water mixture in the organic matter-clay mineral composite pore system of lacustrine shales: a case study of the Da'anzhai member of the Jurassic Ziliujing formation, Sichuan basin. Oil Gas Geol. 46, 304–314. https://doi.org/10.11743/ogg20250121.
Rykov, S.V., Kudryavtseva, I.V., Rykov, S.A., 2023. Saturation line of ethane in the renormalization group theory using the Clapeyron–Clausius equation. Russ. J. Phys. Chem. A 97, 2367–2378. https://doi.org/10.1134/S0036024423110286.
Su, A., Zhang, S., Han, D., et al., 2004. Behavior of chain alkane molecular components in PVT fractionation experiment. Acta Sedimentol. Sin. 22, 354–358. https://doi.org/10.3969/j.issn.1000-0550.2004.02.024 (in Chinese).
Su, A., Xiang, L., 2000. Effect of phase-controlled and gas-wash fractionation on variation of component and carbon isotope composition of oil and gas. Geochimica 29, 549–555 (in Chinese).
Sun, Z., Chen, J., Jia, W., et al., 2025. Geochemical characteristics of light hydrocarbons generated in thermochemical sulfate reduction: results from three series of simulation experiments. Mar. Petrol. Geol. 177, 107388. https://doi.org/10.1016/j.marpetgeo.2025.107388.
Thompson, K.F.M., 1987. Fractionated aromatic petroleums and the generation of gas-condensates. Org. Geochem. 11, 573–590. https://doi.org/10.1016/0146-6380(87)90011-8.
Thompson, K.F.M., 1988. Gas-condensate migration and oil fractionation in deltaic systems. Mar. Petrol. Geol. 5, 237–246. https://doi.org/10.1016/0264-8172(88)90004-9.
Tuo, J., 2002. Research status and advances in deep oil and gas exploration. Adv. Earth Sci. 17, 565–571. https://doi.org/10.3321/j.issn:1001-8166.2002.04.016 (in Chinese).
Wang, Q., Deng, H., Mo, T., et al., 2024. Carbon and hydrogen isotopic compositions of C_7 hydrocarbons and their geochemical significance in light oils/condensates from the Kuqa depression, Tarim Basin, NW China. Org. Geochem. 192, 104783. https://doi.org/10.1016/j.orggeochem.2024.104783.
Wever, H.E., 2000. Petroleum and source rock characterization based on C_7 star plot results: examples from Egypt. AAPG Bull. 84, 1041–1054. https://doi.org/10.1306/a9673ba8-1738-11d7-8645000102c1865d.
Wu, H., Lai, Q., Feng, Z., et al., 2025. Progress on key technologies for logging evaluation of deep and ultra-deep carbonate reservoirs. Earth Sci. 50 (7), 2844–2860. https://doi.org/10.3799/dqkx.2025.116 (in Chinese).
Xiao, Q., Sun, Y., Chai, P., 2011. Geochemical characterization of light hydrocarbons and its controlling factors in Carboniferous crude oils from the TZ4 Oilfield, Tarim Basin, NW China. Acta Geol. Sin. 32, 206–211. https://doi.org/10.7623/syxb201102003 (in Chinese).
Xiao, Q., Sun, Y., Zhang, Y., et al., 2012. Stable carbon isotope fractionation of individual light hydrocarbons in the C_6–C_8 range in crude oil as induced by natural evaporation: experimental results and geological implications. Org. Geochem. 50, 44–56. https://doi.org/10.1016/j.orggeochem.2012.06.003.
Zhang, G., Ma, F., Liang, Y., et al., 2015. Domain and theory-technology progress of global deep oil & gas exploration. Acta Geol. Sin. 36, 1156–1166. https://doi.org/10.7623/syxb201509015 (in Chinese).
Zhang, H., Xu, J.B., Zhang, K., et al., 2020. Geochemical characteristics of carbon and hydrogen isotopes of light crude oils from the deep reservoirs in the Tazhong area of Tarim Basin, NW China. Petrol. Sci. Technol. 38, 509–515. https://doi.org/10.1080/10916466.2020.1767133.
Zhang, S., Huang, H., 2005. Geochemistry of Palaeozoic marine petroleum from the Tarim Basin, NW China: part 1. Oil family classification. Org. Geochem. 36, 1204–1214. https://doi.org/10.1016/j.orggeochem.2005.01.013.
Zhang, S., Su, J., Wang, X., et al., 2011. Geochemistry of Palaeozoic marine petroleum from the Tarim Basin, NW China: part 3. Thermal cracking of liquid hydrocarbons and gas washing as the major mechanisms for deep gas condensate accumulations. Org. Geochem. 42, 1394–1410. https://doi.org/10.1016/j.orggeochem.2011.08.013.
Zhang, Z., Wang, H., Zhu, G., et al., 2022. Phase fractionation and oil mixing as contributors to complex petroleum phase in deep strata: a case study from LG7 block in the Tarim Basin, China. Mar. Petrol. Geol. 140, 105660. https://doi.org/10.1016/j.marpetgeo.2022.105660.
Zhu, G., Li, J., Zhang, Z., et al., 2020. Stability and cracking threshold depth of crude oil in 8000 m ultra-deep reservoir in the Tarim Basin. Fuel 282, 118777. https://doi.org/10.1016/j.fuel.2020.118777.
Zhu, Y., Zhang, Y., Zhao, X., et al., 2022. The fault effects on the oil migration in the ultra-deep Fuman oilfield of the Tarim Basin, NW China. Energies 15, 5789. https://doi.org/10.3390/en15165789.